Laboratory verification on waveform inversion of an internal solitary wave in the South China Sea

M.-H. Cheng, and John R.-C. Hsu
National Sun Yat-sen University
70 Lienhai Rd.
Kaohsiung 80424, Taiwan

Abstract- While shoaling from deepwater in a stratified ocean, an internal solitary wave may undergo waveform inversion on a continental margin. Although many oceanographers have believed the inversion from depression to elevation may commence at the turning point where the upper and low layer equals in depth, this phenomenon has not been fully verified in field observations or numerical schemes. In order to clarify this unique phenomenon, a series of laboratory experiments were conducted on the evolution of an interfacial solitary wave of depression across a slope following by a horizontal plateau similar to a slope-shelf topography. Experimental results indicate that the process of waveform inversion took place after internal run-down, hydraulic jump, vortex motion and run-up on the front slope. Shoaling effect on the horizontal plateau then further dissipated wave energy.

I. Introduction

Like many topographically semi-enclosed seas in the world, the South China Sea (SCS) is abundant in internal solitary wave (ISW) activity. A large ISW affects not only oil drilling operations [1], produces turbulent mixing [2], but also causes nutrient pumping and induces fish forage [3]. In the SCS, a depression ISW with amplitude up to 170 m was observed with the velocity difference between the upper and lower layer exceeding 2.4 ms^{-1} [4]. As an ISW propagates westward across the Luzon Strait between Taiwan and the Philippines, which has a complex topography (Fig. 1), part of its energy may dissipate by vertical vortices and internal turbulent mixing on the continental shelf near Dongsha Island, where the average slope is about 30° in the depth of 150 ~ 200 m. The consequence of nutrient pumping and pollutant resuspension may have affected the ecological environment for the coral reefs in the northeast of the island [5].

Many oceanographers concur that the waveform of a depression ISW may invert as the wave propagates from deep to shallow water. The action commences at the turning point where the upper layer (h_1) and the lower layer (h_2) are equal in depth. An ISW in depression becomes unsettled once it enters the shallow water where $h_1 > h_2$; and eventually transforms into an elevation internal wave (IW) with a favorite depth ratio. Some researchers used a Transitional KdV approach [7] or KdV theory with cubic nonlinearity to calculate the evolution of an ISW passing a turning point [8]. However, the process of waveform inversion cannot be dealt with by an analytical approach in Eulerion form which is conventionally limited to non-breaking waves. Based on a series of SAR imageries, Hsu and Liu [9] presented a collective picture showing the spatial distribution of many large ISWs in the northern SCS in the 1990s to early 2000s (Fig. 2). From the successive order of the bright and dark bands on the imagery, the existence of waveform inversion was postulated, which suggested that a depression ISW had bright band ahead of dark band and an elevation ISW with dark band leading a bright one.

More recently, some researchers [10] recorded ISW motions using moored acoustic instruments on the continental shelf site (with slope-shelf topography) in the northern SCS and found large internal waveform evolution as it entered shallow water from the shelf edge (Fig. 3). As the wave approached the shelf edge from a location about 4.5 km away, where the depth of the mooring site was about 116 m, waveform became asymmetric and reduction in amplitude was detected. In general, satellite imagery offers an indirect means for identifying the existence of waveform inversion, while other advanced field equipments can only deliver an instant imagery at a fixed point rather the spatial process of waveform inversion. Both provide no quantitative information (e.g., variation in wave amplitude, wavelength and energy dissipation) for the overall wave evolution, not to mention the waveform inversion from depression to elevation; hence a plausible alternative is necessary for studying this important oceanographic feature.

In order to overcome the limitations mentioned above, numerous numerical models have been attempted to study the evolution of an ISW propagating on a slope-shelf topography [11], [12], [13]. Amongst these, Vlasenko and Hutter [11] used a numerical scheme to simulate the breaking of an ISW over a slope-shelf topography, and suggested the conditions for the occurrence of a breaking event. Despite a waveform inversion process can be modeled by a numerical method, most works have focused on the evolution of density mixing and overturning on the front slope, without investigating the propagation on the plateau of a slope-shelf topography.

The aim of this paper is to discuss the evolution of waveform inversion based on the results of a series of laboratory experiments using an ISW of depression propagating from a relatively deeper section across a trapezoidal obstacle, which had a horizontal plateau where the upper layer was larger than the bottom layer in order to facilitate the physically existence of an elevated IW. The

978-1-4244-5222-4/10/$26.00 ©2010 IEEE

results demonstrate the inversion of a depression ISW into elevation on the horizontal plateau beyond a turning point. Detailed examination also includes the influence of inversion on the wave amplitude, phase speed and energy of the inverted new wave across the plateau.

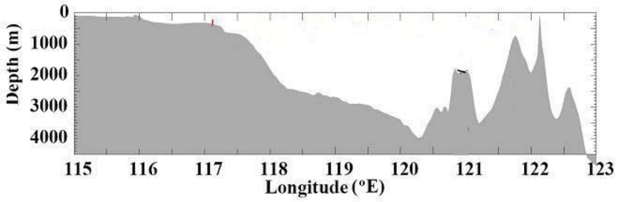

Figure 1 A transect showing the distorted variable topography consisting of ridges in the Luzon Strait and continental shelf-slope to the west in the northern SCS [6].

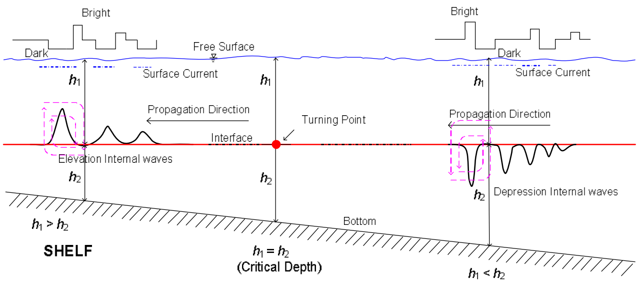

Figure 2 Hypothetical sketch showing waveform inversion of an internal wave after reaching a turning point on a continental shelf [8].

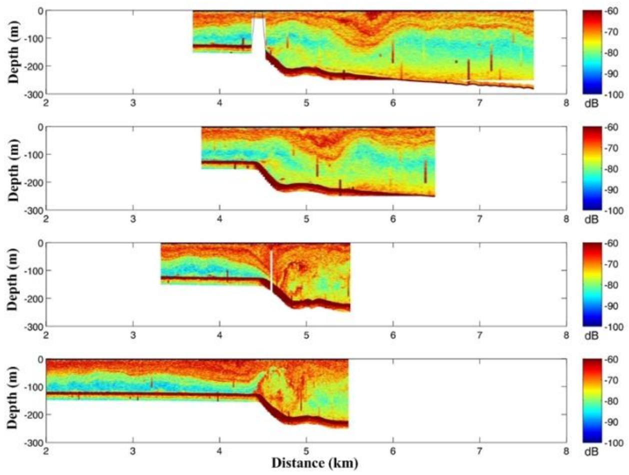

Figure 3 Spatial variations in acoustic backscatter images collected from four repeated transects across one internal wave, with the first on the top panel and the last at the bottom [9].

II. Experimental Apparatus

In the laboratory experiments, a depression ISW was produced in a stratified two-layer fluid system within a steel-framed wave tank 12 m long, 0.7 m high by 0.5 m wide at the National Sun Yat-sen University in Taiwan. The fluid density in the upper (fresh) and lower (brine) layers was 996 and 1030 kg/m^3, respectively. The experimental apparatus, including the shelf-slope topography, five ultrasonic probes and other recording devices, are illustrated in Fig. 4. A shelf-slope topography made of smooth impermeable acrylic (0.37 m high and 6.3 m long), had a horizontal plateau 4.8 m long and front slope with 1.5 m in horizontal projection. The front toe was located near the middle of the tank where the total water depth H (= h_1+h_2) was 0.55 m in all the experiments. In order to study the inversion, the depth of upper layer larger than that of the lower layer was purposely arranged on the plateau. A total of 23 runs were performed (Table 1). An ISW was generated by a "collapse" mechanism arising from the difference in the interface level on either side of a vertical sluice gate, which when opened produced the overturning of the water column and induced required ISW. The relative difference in the water depth between the upper and lower layer (i.e., step depth η_0; see Fig. 4) and initial ISW amplitude (a_1) were two of the main input parameters.

During the experiments, probe 1 recorded the amplitude of the incident ISW; probes 2 and 3 measured the waveform of the ISW on the front slope of the trapezoidal obstacle; while probes 4 and 5 measured the evolution of the transmitted wave above the horizontal plateau. Dyes were injected at selected locations to aid in flow visualization and observation of the mixing process of the ISW propagating over the trapezoidal obstacle. The fluorescent red and blue dyes which had densities of 1011 and 1020 kg/m^3, respectively, floated in the upper and lower layers.

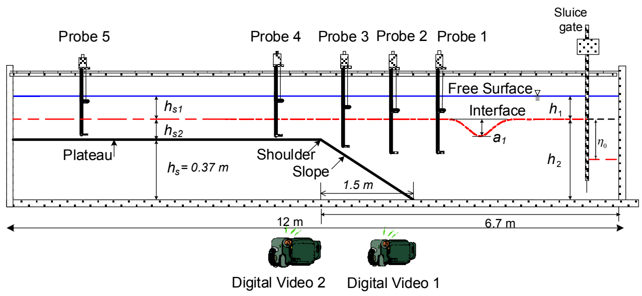

Figure 4 Schematic diagram showing experimental set-up for studying waveform inversion of a depression ISW.

Table 1 Summary of water depths and incident amplitude in the stratified two-layer system shown in Fig. 4

h_1 (cm)	h_2 (cm)	h_{s1}(cm)	h_{s2}(cm)	a_1 (cm)
10	45	10	8	2~5
13	42	13	5	2~5
14	41	14	4	2~5
15	40	15	3	2~5

III. Evolution of a Depression ISW over a Trapezoidal Obstacle

A. Wave Evolution on the Front Slope

As a depression ISW propagating toward a trapezoidal obstacle, its leading trough encountered the front slope first, prior to across the shoulder, then onto the horizontal plateau. With large incident amplitude (a_1),of the ISW intense breaking and vortex motion were observed on the front slope. The former was a phenomenon consisting of the lowering of the interface level above the upper reach of the slope, draw-down of the brine water from the bottom layer on the horizontal plateau and debauching across the shoulder, together with internal hydraulic jump, turbulent mixing and subsequent run-up along the slope. Finally, waveform inversion occurred at the leading edge of the plateau. One of such photographic examples is illustrated in Fig. 5 (each frame in the background was 5 x 5 cm) for an incident ISW propagating across a horizontal plateau of 4.8 m long, with the thickness of the upper layer (h_{s1} = 0.13 m) greater than the bottom layer (h_{s2} = 0.05 m) above it. The turning point in this arrangement was near the quarter point from the shoulder directly above the front slope, and the water depth ratio above the plateau helped sustain the existence of an elevated waveform.

While the depression ISW propagating on the slope (Figs. 5a~5b), it first caused a draw-down of fluid from the bottom layer on the plateau (Fig. 5c) and a depression waveform remained near the turning point (at probe 3 position shown in Fig. 4). The draw-down action carried more fluid across the shoulder downward along the slope and reduced the thickness of the bottom layer at the upper reach of the slope (Figs. 5c~5d), until the interface reached a lowest level (Fig. 5e). During this time, the above process triggered the onset of an internal hydraulic jump (Fig. 5f) near the turning point, followed by a bore-like vortex surging up along the upper reach of the slope toward the shoulder (Figs. 5f~5g). When the bore reached the shoulder (Fig. 5g), it raised the level of the interface as the wave continued spreading across the plateau and a secondary oscillation formed at its trailing end (Fig. 5h). The latter was produced by two vortices on the upper reach of the slope induced by the velocity difference between the upper and bottom layer produced, with a clockwise vortex resulting from the internal hydraulic jump beneath the other counterclockwise vortex induced by gravity instability. When the bore climbed up the slope, the clockwise vortex dissipated swiftly. Consequently, the bore associated with the counterclockwise vortex evolved into a clockwise vortex by the stress reversal induced by the velocity field within the bottom layer. Finally, an elevation-like internal wave (IW) emerged, and propagated onto the plateau (Fig. 5i), further downstream along it (Fig. 5j).

B. Waveform Evolution on Horizontal Plateau

When an elevated waveform propagated across the horizontal plateau where the upper layer was thicker than the bottom layer, the amplitude of its trough reduced, while its crest increased. The process of waveform evolution on the plateau is highlighted in Fig. 6 (again, each background frame was 5 x 5 cm). The level of original interface had been dropped as the leading front of a depression ISW approaching the plateau (Figs. 5g and 6a). Whilst propagating into the plateau (Fig. 6b), the original depression waveform almost disappeared, the bolus consolidated from a double hump into single shape (Fig. 5h~5i) and an elevation-like IW resulted (Fig. 6c). As the leading wave front passed the shoulder and was entering the plateau, the interface level increased. As this new waveform propagated further along the plateau, it might suffer energy dissipation due to bottom friction (Fig. 6d).

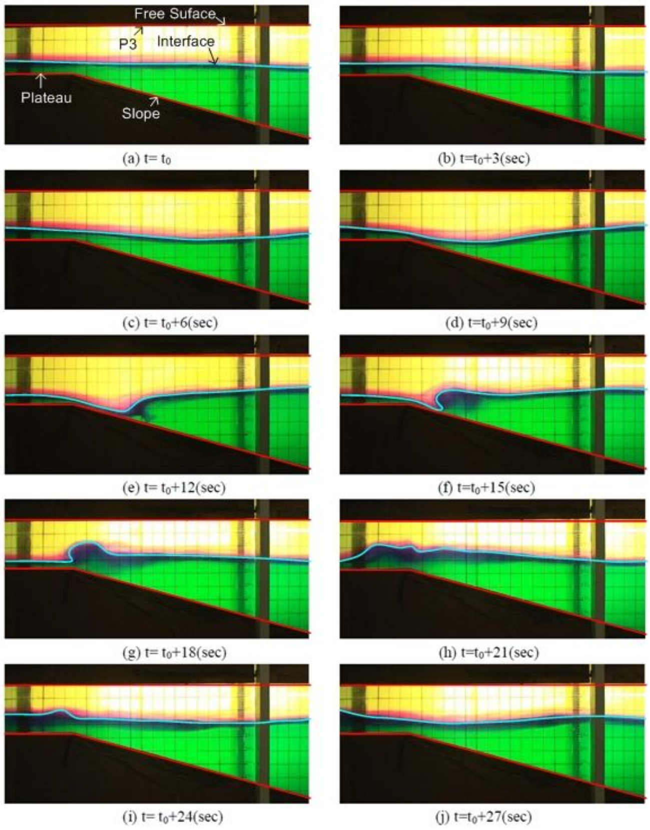

Figure 5. Sequence of events showing an ISW of depression across a trapezoidal obstacle. (Experimental conditions - see Fig. 4 for notations: h = 0.13 m, h_2 = 0.42 m, h_s = 0.37 m, a_1 = 0.043 m)

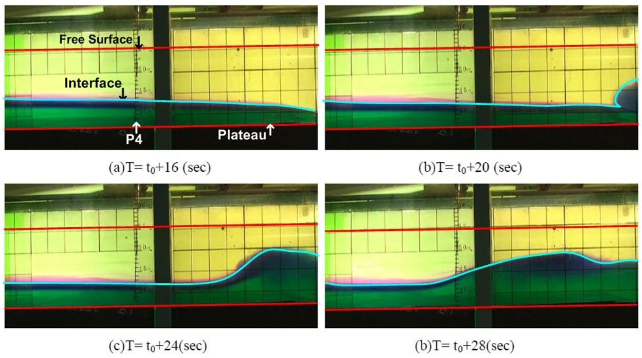

Figure 6. Sequence of events showing the propagation of an ISW of depression propagating over a trapezoidal obstacle. (Experimental conditions: H_1 = 0.13 m, H_2 = 0.42 m, h_s = 0.37 m, a_1 =0.043 m)

C. Time Series of Waveform Profiles for all Five Probes

In order to study the waveform evolution, the process can be observed from the recorded wave profiles (Fig. 7) at the five ultrasonic probe locations shown in Fig. 4. Initially, the leading waveform of the incident ISW at probe 1 was dominated by depression (trough) and it remained in depression above the toe of the front slope (probe 2). The waveform indicated by the wave profiles at probes 4 and 5 was mainly in elevation type, while probe 3 showed an ISW of depression with increasing strength of elevation at the trailing end. It may be concluded that this waveform inversion (from probe 3 to probe 4) was generated after the turning point despite the occurrence of wave breaking. Overall, the process of waveform inversion and generation of a new wave of elevation-type occurred in two steps: First, through turbulent mixing and the formation of a strong vortex on the slope; and second, by shoaling and propagating along the horizontal plateau where the upper layer was thicker than the lower layer. Upon comparing the images in Fig. 5 and waveform profiles in Fig. 7, the waveform at probe 3 had unusual waveform consisting of an elevated bolus together with a large trough in depression. This process could provide extra energy input to the subsequent wave evolution on the plateau.

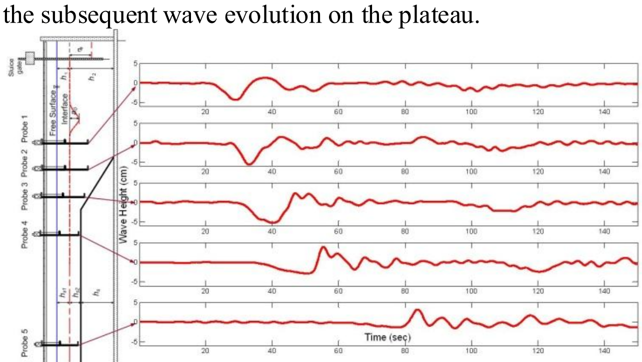

Figure 7 Time series of ISW profiles recorded by ultrasonic probes at five locations along a wave tank. (Experimental conditions: $h_1 = 0.14$ m, $h_2 = 0.41$ m, $h_s = 0.37$ m, $a_I = 0.05$ m; see Fig. 4 for notation)

IV. RESULTS AND DISCUSSION

Dimensionless parameters for wave amplitude, group speed and energy are defined and their values calculated from the recorded wave profiles for further analysis on waveform inversion. The amplitude of each wave crest or trough is calculated using the maximum or minimum of each leading wave component in the records (e.g. Fig. 7). By relating the amplitude of the crest to trough at each probe location, the dimensionless amplitude ratios (A_{t1}, A_{t2}, A_{t4} and A_{t5}; see (1) ~ (4) below) can help indicate the wave type at each location. For example, $A_{ti} = 1$ (i = 1, 2, 4, 5) implies equal amplitude of crest to trough, $A_{ti} > 1$ for crest greater than trough, and $A_{ti} \ll 1$ for an almost complete depression waveform. Furthermore, the non-dimensional incident amplitude or relative incident wave amplitude (α) related to the thickness of the bottom layer above the horizontal plateau is used in (5); while (6) and (7) denote the relative transmitted wave amplitude (T_A) and transmitted energy (T_E), respectively, at the down drift end of the journey at probe 5 for the physical properties in relation to the incident wave conditions.

$$A_{t1} = a_{1+} / a_{1-} \tag{1}$$
$$A_{t2} = a_{2+} / a_{2-} \tag{2}$$
$$A_{t4} = a_{4+} / a_{4-} \tag{3}$$
$$A_{t5} = a_{5+} / a_{5-} \tag{4}$$
$$\alpha = a_{1-} / h_{s2} \tag{5}$$
$$T_A = a_{5+} / a_{1-} \text{ or } a_{5-} / a_{1-} \tag{6}$$
$$T_E = E_{5+} / E_{1-} \text{ or } E_{5-} / E_{1-} \tag{7}$$

In (1)~(7) above, a_{1+}, a_{1-}, a_{2+}, a_{2-}, a_{4+}, a_{4-}, a_{5+} and a_{5-} are the amplitude of the crest or trough of the leading waveform at probes 1, 2, 4 and 5, respectively (with the vertical z-axis positive upwards from the original interface); h_1 and h_2 are the depth of the upper layer and bottom layer at probe 1 location (see Fig. 4), h_s is the vertical height of the trapezoidal obstacle, and h_{s1} and h_{s2} denote the thickness of the upper and bottom layer above the horizontal plateau. The wave energy (E) defined by Michallet and Ivey [14] for the trough of a depression wave (Fig. 8(a)) is now extended to the complete wave profile of trough to crest (as conventionally employed in dealing with surface gravity waves, Fig. 8(b)) in order to study ISW waveform inversion from depression to elevation:

$$E = Cg\triangle\rho \int_{t2}^{t1} \eta^2(t)\ dt \tag{8}$$

In (8), a_i is the amplitude of each leading ISW at each location to be analyzed, C the wave phase speed, g the acceleration due to gravity, η the temporal interface level of the wave motion, and $\triangle\rho = \rho_2 - \rho_1$, where ρ_1 and ρ_2 are the fluid density of the upper and bottom layer, respectively. The difference in time, $t_1 - t_0$, is termed as characteristic period (P_w), calculated from a leading wave profile at two consecutive time steps t_1 and t_0 for the first and second zero-down crossing points on a wave record. Subscripts – and + are used to denote the trough and crest components, respectively.

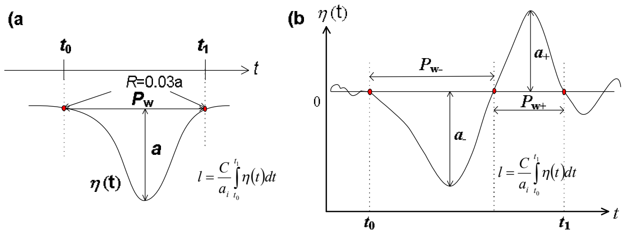

Figure 8. Definition sketch for characteristic wave period (P_w) in (a) depression ISW in [14], and (b) complete waveform of trough to crest using zero-down crossing between two consecutive time steps (t_1 and t_0) in the present study; showing also the definition of characteristic wavelength (l).

A. Waveform Inversion

The likelihood of waveform inversion as a depression ISW propagates over a slope-shelf topography can be determined from the ratio between dimensionless amplitude α versus characteristic amplitude at crests and troughs. The ratios recorded at probes 1, 2, 4 and 5 (A_{t1}, A_{t2}, A_{t4} and A_{t5}) are used to compile the picture seen in Fig. 9. The symbols (circles, triangles, stars and rectangles) indicate the values of wave amplitude recorded at probes 1, 2, 4 and 5, respectively. In all the 23 runs, the dimensionless amplitude $A_{t1} < 0.5$ at probe 1 was indicative of the incident ISW in depression. Under different conditions, the waveform evolved differently as a depression ISW propagated over the slope-shelf topography, depending on the ratio of water depth between the upper (h_{s1}) and lower (h_{s2}) layers. A comparison on the results of A_{t4} and A_{t5} shows that the phenomenon of waveform inversion had almost taken place at probe 5, but not always at the position of probe 4.

A closer examination on the results shown in Fig. 9 suggests $\alpha = 0.3$ can be used to demarcate the occurrence of waveform inversion; and $\alpha = 0.7$ to distinguish the runs with waveform inversion induced by shoaling effect and intense wave breaking. In addition, shoaling effect played a major role in waveform inversion within the range of $0.3 < \alpha < 0.7$. When $\alpha > 0.7$, a new elevation-like IW would generate resulting from a series of process, consisting of run-down, internal hydraulic jump, strong vortex and run-up, which led to waveform inversion (described in section III. A). Although the phenomenon of waveform overturning at the trailing part of the waveform was observed, as well as shoaling effect and the depth ratio was favorable to support an elevated IW, only weak waveform inversion was found away from the turning point for an incident depression ISW with a small $\alpha < 0.7$. In contrast, for a large incident wave, the dynamic of the new IW created a waveform inversion near the turning point as the ISW propagated over the same topography. It is worth noting that the location of the turning point varied slightly depending on the relative depths between the upper and lower layers above the horizontal plateau and the fronting slope.

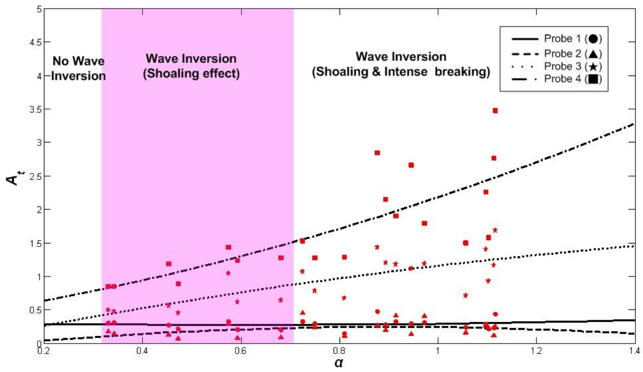

Figure 9 Time series of ISW profiles recorded by ultrasonic probes at five locations along a wave tank. (Experimental conditions: $h_1 = 0.14$ m, $h_2 = 0.41$ m, $h_s = 0.37$ m, $a_1 = 0.05$ m; see Fig. 4 for notation)

B. Variation in Crest and Trough Height

Although the variation of the crest to trough ratio at each probe position can be realized on the horizontal plateau (e.g., Fig. 7), the magnitude of waveform inversion related to incident amplitude in depression cannot be assessed using the relationship between A_t at each probe position and relative incident wave parameter (α) shown in Fig. 9. Alternatively, transmitted amplitude (T_A) at probe 5 versus relative incident amplitude (α) is taken (Fig. 10). The transmitted T_A for the trough (o) of the leading wave decreased as α increased, due to excessive energy dissipation arising from wave breaking on the slope and shoaling along the plateau. On the other hand, T_A for the crest (△) of the leading wave increased as α increased. Within the data range of α = 0.2 and 1.2, the transmitted amplitude ratio for trough (T_{A-}) decreased from 0.65 to 0.25 on the horizontal plateau, while that for the crest (T_{A+}) increased from 0.45 to 0.72, which was about 66% of that lost from the trough. Despite the increase in the transmitted T_{A+} for the crest and the decrease in T_{A-} for the trough while an elevated waveform evolved across the plateau, there was a time when both were equal in amplitude. This can be found from the intersection of the two regressed lines (red circle in Fig. 9), at a critical value of $\alpha_{crit} = 0.44$.

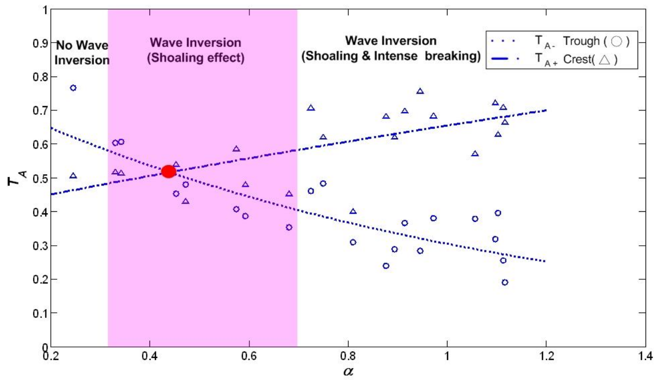

Figure 10. Calculated transmitted amplitude (T_A) at probe 5 versus relative incident amplitude (α) across a plateau. Colored hatch denoting waveform inversion due to shear effect within $0.3 < \alpha < 0.7$.

C. Variation in Transmitted Phase Speed

In addition to the amplitude of the leading wave, the variability in phase speed was another important property as an ISW propagated over the trapezoidal obstacle with a horizontal plateau. The magnitude of wave phase speed (V_1, V_2 and V_3) can be calculated for each of the three sectors between probes 1, 2, 4 and 5, respectively. By plotting their values (V_1, V_2 and V_3) versus relative incident amplitude (α) for all experimental runs (Fig. 11), the relative strength of the flow field can be compared throughout the entire process of evolution for the wave propagation. Whilst the wave propagated across the horizontal plateau, the incident phase speed V_1 between probes 1 and 2 was the highest, and that on the early reach of the plateau (V_2) between probes 2 and 4, was the slowest, while that between probes 4 and 5 (V_3) between them. Based on the results for each α value in Fig. 11, it may be envisaged that wave speed of the leading wave (V_3) decreased due to bottom friction whilst it propagated on the plateau compared to the initial V_1. On the other hand, as the wave across the front slope and shoulder, a series of factors (including draw-down, internal hydraulic jump, intense vortex and run up) might have reduced the speed (V_2) significantly and its value was not affected by the increase of α, in spite of the increase in V_1. In addition, the phase speed of the transmitted wave (V_3) only increased marginally, regardless of the increase of incident amplitude.

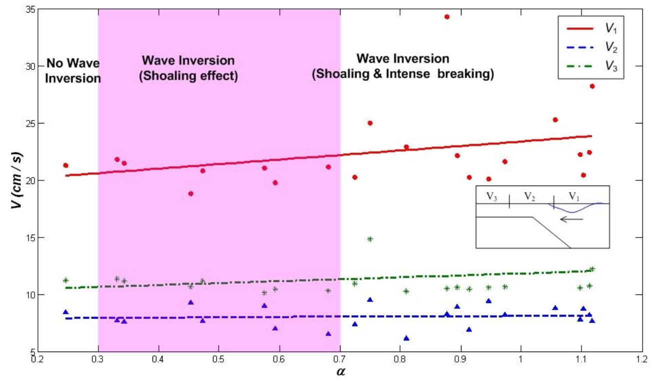

Figure 11. Calculated wave phase speeds (V_1, V_2 and V_3) for the three sectors between probes 1, 2, 4 and 5 versus relative incident amplitude (α). Data from the present study

D. Variation in Transmitted Wave Energy

Beside the variation in the transmitted wave amplitude (e.g., Fig. 10) and phase speed (Fig. 11), energy is calculated using (8) from the wave profile recorded by probe 5, from which energy dissipation of the leading wave can be obtained. By plotting the relative transmitted energy (T_E) at probe 5 versus the relative incident amplitude (α) as in Fig. 12, a generally rapid decreasing trend for the wave energy associated with the trough can be appreciated on the plateau, as an elevated waveform propagating above it. As α increased, the resultant energy for the crest (T_{E+}) and trough (T_{E-}) at probe 5 location had a slow increasing trend, due to the fact that large portion of the energy dissipation was associated with intense wave breaking on the front slope, and the consolidation of the elevated IW above the plateau on which its upper layer was greater than the bottom layer. Interestingly, as α increased, energy for the crest (T_{E+}) on the plateau did not increase proportional to the square of the amplitude, perhaps because a large amount of the energy had lost due to intense breaking on the front slope.

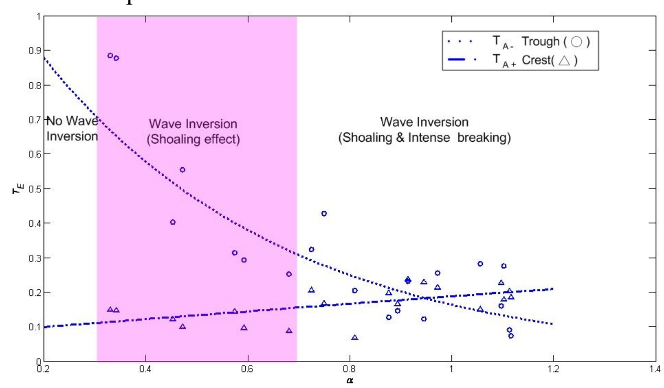

Figure 12. Transmitted relative energy (T_E) at probe 5 versus relative incident amplitude (α) across a horizontal plateau. Colored pattern for waveform inversion due to shear effect within 0.3 < α < 0.7.

E. Variation in Transmitted Wave Period

Whilst a depression ISW encountered a submarine obstacle (e.g., ridge or shelf), the fundamental frequency of the leading wave observed in field condition [15] was found to shift from low to high value (from long to short period). Although the frequency variability was identified, the process of frequency evolution had never been quantified, particularly for that related to waveform inversion. In order to study the variations in the period associated with waveform inversion, the HHT method [16] is used to analyze the time series data recorded by four ultrasonic probes in the present laboratory experiments. A record with time interval of 40 sec was taken from in each record.

The outputs of marginal spectrum and time-frequency and energy spectrum from HHT at four probe locations (1, 2, 4 and 5) are given in Fig. 13 and Fig. 14, respectively. In Fig. 13, the frequency increased from 19.95 s at (P1) to 26.30 s (P2), and increased further to 31.62 s at P4, following by conspicuous reduction to 8.32 s at P5. This implies that the wave period of a depression ISW reduced from 19.95 to 8.32 seconds. A close examination of Fig. 14 finds that, from P1 to P5, the frequency band shifted from log 1.3~1.6 s to log 0.9~1.4 s, indicating the down-shift of the active wave period, with center around log 4.4 s at P2 and P4. Comparing the four sub-plots in Fig. 13 for the fundamental frequency of the incident ISW, this frequency shift into shorter period band associated with the new ISW of elevation was obvious. Again, the marginal spectrum of P1 and P5 in Fig. 13 suggests energy of the leading wave suffered a significant dissipation when it propagated across a trapezoidal obstacle.

V. CONCLUSIONS

The laboratory study on the propagation of a depression ISW over a trapezoidal obstacle help understand the process of waveform evolution over a shelf-slope topography in field condition. Employing the water depth of the upper layer greater than the lower part on s horizontal plateau, waveform inversion became apparent on a shelf-slope topography. In all the 23 runs examined, the phase speed decreased significantly toward the shoulder of the shelf-slope, especially after a strong vortex on the upper reach of the slope, which consequently triggered wave inversion. In addition, the transmitted wave amplitude, wave speed and wave energy were influenced by the depth ratio between the upper and lower layers above the horizontal plateau.

As a depression ISW shoaled from deepwater, waveform inversion could be observed on the plateau, under favorable depth condition. However, the mechanism responsible for promoting waveform inversion depended mainly on the magnitude of the dimensionless amplitude α. For a large incident ISW of depression, an elevation IW could be generated by the combined effects of interface draw-down, internal hydraulic jump, vortex, turbulent mixing and run-up on the front slope. On the other hand, for a depression ISW in small amplitude, waveform inversion was controlled by shoaling effect. In both cases, waveform commenced inversion from depression into elevation around the turning point. Moreover, most of the incident energy was dissipated as the newly generated elevation-like IW propagated across the horizontal plateau, accompanying by the frequency shift from long wave period to short period.

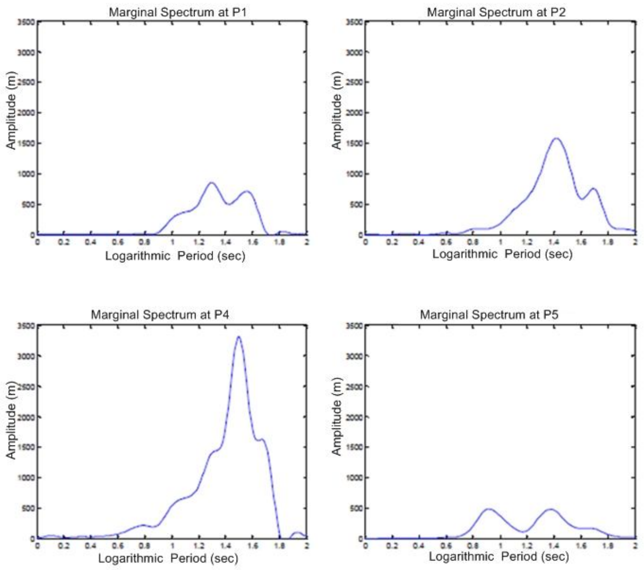

Figure 13 Marginal spectrum calculated by HHT at four probe locations along a wave tank. (Experimental conditions: $h_1 = 0.14$ m, $h_2 = 0.41$ m, $h_s = 0.37$ m, $a_1 = 0.05$ m; see Fig. 4).

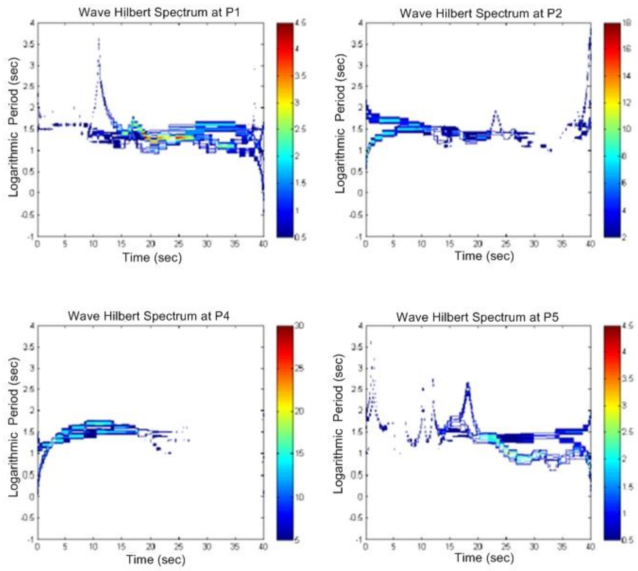

Figure 14 Time-frequency and energy patterns calculated by HHT at four probes along a wave tank. (Experimental conditions: $h_1 = 0.14$ m, $h_2 = 0.41$ m, $h_s = 0.37$ m, $a_1 = 0.05$ m; see Fig. 4).

ACKNOWLEDGMENT

The authors acknowledge the support to JRCH from the National Science Council of the Republic of China, under grant No. NSC 97-2611-M-110-013 and also from Asia-Pacific Ocean Research Center (APORC) in the National Sun Yat-sen University. They also wish to thank the assistance of Dr. H. Michallet, Laboratoire des Ecoulements Géophysiques et Industriels (LEGI), Institute National Polytechnique de Grenoble, France for the acquisition of the ultrasonic probes used in the experiments.

REFERENCES

[1] J.B. Bole, J.J. Ebbesmeyer, and R.D. Romea, “Soliton currents in South China Sea: measurements and theoretical modeling,” [Proceedings of 26th Annual Offshore Technology Conference, Houston, Texas, pp. 367-375, 1994]

[2] J.N. Moum, D.M. Farmer, W.D. Smyth, L. Armi, and S. Vagle, “Structure and generation of turbulence at interfaces strained by internal solitary waves propagating shoreward over the continental shelf,” Journal of Physical Oceanography, vol. 33, pp. 2093-2112, 2003.

[3] J.E. Corredor, “Development and propagation of internal waves in the Mona Passage,” Sea Technology, vol. 49 (10), pp. 48-50, 2008.

[4] A. Warn-Varnas, J. Hawkins, K.G. Lamb, S. Piacsek, S. Chin-Bing, D. King, and G. Burgoes, “Solitary wave generation dynamics at Luzon Strait,” Ocean Modelling, vol. 31, pp. 9-27, 2010.

[5] Y.H. Wang, C.F. Dai, and Y.Y. Chen, “The physical and ecological processes of internal waves on an isolated reef ecosystem in the South China Sea,” Geophysical Research Letters, vol. 34, L18609, doi:10.1029/2007GL030658, 2007.

[6] Y. Niwa, and T. Hibiya, “Three-dimensional numerical simulation of M2 internal tides in the East China Sea,” Journal of Geophysical Research, vol. 109, pp. C04027, doi:10.1029/2003JC001923, 2004

[7] C.J. Knickerbocker, and A.C. Newell, “Internal solitary wave near a turning point,” Physical Letters, vol. 75A(5), pp. 326-330, 1980.

[8] K.R. Helfrich, and W.K. Melville, “On long nonlinear internal waves over slope-shelf topography,” Journal of Fluid Mechanics, vol. 167, pp. 285-308, 1986.

[9] M.K. Hsu, and A.K. Liu, “Nonlinear internal waves in the South China Sea,” Canadian Journal of Remote Sensing, vol. 26, pp. 72-81, 2000.

[10] D.B. Reeder, T.F. Duda, and B. Ma, “Short-range acoustic propagation variability on a shelf area with strong nonlinear internal waves,” Ocean 2008 - MTS/IEEE Kobe Techno-Ocean, vol. 1-3, pp. 65-172, 2008.

[11] V. Vlasenko, and K. Hutter, “Numerical experiments on the breaking of solitary internal waves over a slope-shelf topography,” Journal of Physical Oceanography, vol. 32 (6), pp. 1779-1793, 2002.

[12] R.J. Small, and R.P. Hornby, “A comparison of weakly and fully non-linear models of the shoaling of a solitary internal wave,” Ocean Modelling, vol. 8, pp. 395–416, 2005.

[13] K.G. Lamb, and V.T. Nguyen, “Calculating energy flux in internal solitary waves with an application to reflectance,” Journal of Physical Oceanography, vol. 39, pp. 559-580, 2009.

[14] H. Michallet, and E. Barthelemy, “Experimental study of interfacial solitary waves,” Journal of Fluid Mechanics, vol. 366, pp. 159-177, 1998.

[15] S.R. Ramp, T.Y. Tang, T.F. Duda, J.F. Lynch, A.K. Liu, C.S. Chiu, F.L. Bahr, H.R. Kim, and Y.J. Yang, “Internal solitons in the northeastern south China Sea. Part 1: sources and deep water propagation,” IEEE Journal of Oceanic Engineering, vol. 29(4), pp. 1157-1181, 2004.

[16] N.E. Huang, Z. Shen, S.R. Long, W.L. Wu, and H.H. Shih, “The empirical mode decomposition and Hilbert spectrum for nonlinear and nonstationary time series analysis,” Proceedings, Royal Society London, Ser. A, vol. 454, pp. 903-995, 1998.